

# ArduSoar: an Open-Source Thermalling Controller for Resource-Constrained Autopilots

Samuel Tabor  
samuelctabor@gmail.com

Iain Guilliard  
Australian National University  
Canberra, Australia  
iainguilliard@gmail.com

Andrey Kolobov  
Microsoft Research  
Redmond, WA-98052  
Andrey.Kolobov@gmail.com

**Abstract**—Autonomous soaring capability has the potential to significantly increase time aloft for fixed-wing UAVs. In this paper, we introduce ArduSoar, the first soaring controller integrated into a major autopilot software suite for small UAVs. We describe ArduSoar from the algorithmic standpoint, outline its integration with the ArduPlane autopilot, and discuss tuning procedures and parameter choices for it.

## I. INTRODUCTION

Autonomous soaring has long been considered for its promise of extending the range and time in the air for Uninhabited Aerial Vehicles (UAVs). These two UAV characteristics are crucial in a range of scenarios from aerial mapping to crop monitoring to package delivery, and are currently limited by a combination of the UAV’s powerplant and the limited energy available onboard. Exploiting the energy of the sun [25] and of the moving air masses, the latter of which is at the focus of our work, have the potential to increase fixed-wing drone range by many times [6]. While there are many atmospheric phenomena that can help an aircraft gain altitude without the help of a motor, the most ubiquitous of them are *thermals*, rising plumes of air generated by certain areas on the ground giving up heat into the atmosphere.

Including the first feasibility study of autonomous thermalling in 1998 [31], researchers have proposed at least 5 approaches to modeling thermals computationally and soaring in them, evaluating these techniques in simulation [30, 17, 26] and in live tests [7, 14]. Each of them has a significant number of intricacies related to implementation and parameter tuning. Since none of the implementations, which were written in different languages and for different platforms and setups, are publicly available, none of these techniques have been properly compared against each other.

This paper introduces and describes the implementation of a soaring controller called *ArduSoar* as part of a popular open-source UAV autopilot system, ArduPilot [1]. ArduPilot can be built to run on many different autopilot hardware platforms, including Pixhawk [4] and Raspberry Pi 3 [5], as well as as a software-in-the-loop simulation. Being part of an open-source project, ArduSoar’s software components can be reused or inspected to serve as an inspiration, basis or benchmark for other soaring controller designs.

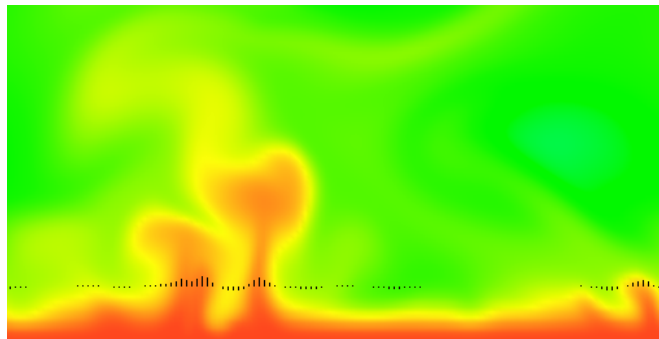


Fig. 1: Rayleigh-Bénard convection simulation showing two rising thermal plumes, with red color indicating hotter air. The lower boundary of the simulation heats the adjacent air hotter than the ambient air temperature. The hotter air gains buoyancy and rises in turbulent plumes to mix with the cooler air above. The small black vertical bars indicate vertical air speed at an altitude and show the typical bell shaped distribution of uplift through the center of a thermal.

## II. SOARING, THERMALS, THERMAL ESTIMATION

Soaring usually refers to process of using a rising air mass to gain altitude by birds and aircraft. Technically, while in *dynamic* soaring the source of lift is a wind gradient [23, 24, 9], not rising air, here we focus on *static* soaring, which always relies on air being pushed upwards in some way.

The most commonly encountered type of rising air regions is a thermal. Thermals start immediately above parts of Earth’s surface that accumulate more heat than surrounding areas and then emit the heat back into the atmosphere, warming up the air above them. Thermals can form over darker terrain, e.g. asphalt or plowed fields, but may also arise above forested and other areas. They are invisible, but are frequently pictured as air columns, possibly slanted due to wind. Vertical air velocity in the center of such a column is higher, becomes lower towards the column fringes, and eventually turns into sink. In reality and even under realistic simulation models, thermals do not always conform to this idealized concept. Figure 1 is a screenshot from a Rayleigh-Bénard simulation (see, e.g., Kadanoff [18]), a standard high-fidelity convection model that gives a more accurate idea of thermals’ irregular and chaotic nature.

In all existing work on autonomous soaring in thermals, autopilots/soaring controllers use thermal models that can be estimated by observing the aircraft’s vertical air velocity and combining this data with information about the aircraft’s 3D position changes. Soaring controllers try to fit such a thermal model to this data and, if the fit is good enough, synthesize a trajectory that exploits the thermal’s lift distribution, as predicted by the model, to gain altitude. The model at the heart of Rayleigh-Bénard simulations has been used in this way to learn sailplane trajectories [26] for simulated aircraft, but is expensive computationally and nontrivial to tune.

Therefore, for computational and ease-of-use reasons, ArduSoar relies on the thermal model proposed by Wharington and Herszberg [31] and modified by Allen and Lin [7]. It makes a number of implicit assumptions, which we make explicit here, all of which apply to *the thermal’s horizontal cross-section at a given altitude*:

- A thermal is stationary: its position and distribution of lift within it, i.e., the air’s vertical velocity, does not change with time. Note, however, that this assumption is for a fixed altitude only, and the model allows for a thermal’s properties to vary with altitude due to air cooling down or due to the thermal getting affected by wind.
- A thermal has a single “center”, called *core*, at position  $x^{th}, y^{th}$ .
- The vertical air velocity within a thermal’s horizontal cross-section has a bell-shaped distribution w.r.t. the thermal core. It is strongest at  $(x^{th}, y^{th})$ , and has speed  $W^{th}$  m/s there. Thus, the lift strength at position  $x, y$  is given by

$$w(x, y) = W^{th} \exp\left(-\frac{(x - x^{th})^2 + (y - y^{th})^2}{R^{th2}}\right), \quad (1)$$

where  $R^{th}$  is a parameter describing the thermal radius.

Parameters  $W^{th}$ ,  $R^{th}$ ,  $x^{th}$  and  $y^{th}$  can be continually estimated using a Kalman filter [20] if we assume a Gaussian distribution over them and keep updating this distribution with sensor observations. Hazard [17] has used an Unscented Kalman filter (UKF) for this purpose. In ArduSoar, due to the computational constraints of the hardware platforms on which it typically runs, Pixhawk and APM, we use an Extended Kalman Filter (EKF) instead.

An EKF is a type of Kalman filter that allows maintaining a Gaussian estimate of the system state given a sequence of observations if the system transition function  $f(\mathbf{X}, \mathbf{u})$  and observation function  $h(\mathbf{X})$  are nonlinear. Specifically, suppose we start with a state distribution  $\mathcal{N}(\mathbf{X}_k, P_k)$ , and want to compute a new estimate  $\mathcal{N}(\mathbf{X}_{k+1}, P_{k+1})$  after a system makes a transition over one time step and we receive an observation  $\mathbf{o}$  about it. To begin with, we linearize of the transition function

$f$  about the current state estimate by computing the Jacobian

$$F = \left. \frac{\partial f}{\partial \mathbf{X}} \right|_{\mathbf{x}_k} \quad (2)$$

Then we update the state estimate using the state transition

$$\hat{\mathbf{X}}_{k+1} = f(\mathbf{X}_k, \mathbf{u}_k) \quad (3)$$

$$\hat{P}_{k+1} = F P_k F^\top + Q \quad (4)$$

Then we linearize  $h$  around this new state estimate by computing the Jacobian

$$H = \left. \frac{\partial h}{\partial \mathbf{X}} \right|_{\hat{\mathbf{x}}_{k+1}} \quad (5)$$

and calculate the approximate Kalman gain

$$K = \hat{P}_{k+1} H^\top (H \hat{P}_{k+1} H^\top + R)^{-1} \quad (6)$$

As the final step, the state distribution so far needs to be corrected for the observation process:

$$\mathbf{X}_{k+1} = \hat{\mathbf{X}}_{k+1} + K(\mathbf{o} - h(\hat{\mathbf{X}}_{k+1})) \quad (7)$$

$$P_{k+1} = (I - KH)\hat{P}_{k+1} \quad (8)$$

Matrices  $Q$  and  $R$  are process and observation noise covariances, respectively, and are tunable parameters in our model.

### III. ALGORITHMIC ASPECTS OF ARDU SOAR

Gaining altitude with a thermal’s help can be broken down into four stages — thermal detection, identification, exploitation, and exit. At an abstract level, an aircraft traveling through the air with its motor shut down will tend to lose altitude at a certain rate that depends on the aircraft’s airspeed via a function called the *polar curve* that we discuss shortly. The autopilot knows both the polar curve and the current airspeed, and therefore at any point can easily determine how fast the aircraft *would be* descending if the air around it was still. If the aircraft is flying through a thermal, the air around it is not still; it is rising and lifting the aircraft with it. The autopilot can detect this by comparing the aircraft’s actual altitude change rate to the one predicted by the polar curve, and enter the thermalling mode. In the thermalling mode, the autopilot continually keeps refitting the altitude change rate data it is receiving to a thermal model, e.g., the model in Equation 1 using an EKF, and trying to keep the aircraft within the thermal to gain altitude. If the altitude change rate becomes close to the “natural” sink rate predicted by the polar curve, it is an indication that the thermal is weak and it is time to exit it. While this reasoning is straightforward, operationalizing it is significantly complicated not only by the inherent uncertainty in thermal parameters but also by the subtleties in attributing the aircraft’s altitude gain to thermal lift as opposed to other factors.

ArduSoar, our soaring controller integrated into an open-source fixed-wing UAV autopilot called ArduPlane [2], overcomes these difficulties and implements the above intuition using the following data streams from ArduPlane’s Attitude and Heading Reference System (AHRS):

- $h$  - altitude
- $\phi$  - roll (bank) angle
- $v$  - airspeed
- $x^{abs}$  - GPS latitude
- $y^{abs}$  - GPS longitude
- $v^{wind}$  - wind velocity

We now describe ArduSoar’s operation in each stage.

#### A. Polar Curve and Variometer Data

The key to ArduSoar’s operation is a stream of *variometer* data, synthesized from data streams described above. To a first approximation, a variometer aims to measure the vertical speed of the air around an aircraft, thereby helping the autopilot determine whether the aircraft is in a thermal. In practice, however, no onboard instrument has direct access to the true vertical speed of the air. A variometer tries to deduce it from the *aircraft’s own* vertical speed w.r.t. the ground, which, in the case of a sailplane with its motor turned off, can be imparted by the sailplane being in a thermal *or* by pitching up or down.

Therefore, instead of measuring the vertical airspeed, we implement a variometer that measures the rate of change of a sailplane’s *total specific energy*. The total energy of a sailplane in a glide (i.e. with the motor off, if present), is

$$E = mgh + \frac{1}{2}mv^2 \quad (9)$$

and the specific energy (in meters) results from dividing through by  $mg$ :

$$e = h + \frac{v^2}{2g} \quad (10)$$

Its rate of change over time is

$$\dot{e} = \dot{h} + \frac{v\dot{v}}{g} \quad (11)$$

Note that the measurement units of  $\dot{e}$  are m/s. Computing variometer data involves estimating  $\dot{h}$  and  $\dot{v}$ , which can be approximated by  $\frac{\Delta e}{\Delta t}$  computed using successive  $h$  and  $v$  data points from the altitude and airspeed data streams.

To recover the true vertical speed of the air mass surrounding the sailplane, we need to further correct  $\dot{e}$  with the aircraft’s natural sink at its current airspeed  $v$  and bank angle  $\phi$ . This corrected variometer is known as a *netto variometer*, and has a value of 0 m/s in a steady glide through still air. The sink rate can be derived from the sailplane’s aforementioned *drag polar curve*. From Anderson [8], the standard simplified formula for the drag polar curve is:

$$C_D = C_{D0} + \frac{C_L^2}{\pi e AR} \quad (12)$$

where  $C_{D0}$  is the *zero lift* drag coefficient,  $AR$  is the aspect ratio and  $e$  is the *span efficiency*, all of which are constants of the airframe. The lift coefficient is defined:

$$C_L = \frac{L}{\frac{1}{2}\rho v^2 S} \quad (13)$$

where  $L$  is the lift force generated by the wings,  $\rho$  is the air density,  $S$  is the wing area, and  $v$  is the airspeed. Since the pitch angle is typically very shallow in a glide, we can approximate  $L \approx W$ , where  $W = mg$ , Which gives:

$$C_L \approx \frac{mg}{\frac{1}{2}\rho v^2 S} \quad (14)$$

and setting  $\mathbf{K} = \frac{2mg}{\rho S^2}$ , which we can assume is a constant for the airframe at least at low altitudes, gives the expression:

$$C_L = \frac{\mathbf{K}}{v^2} \quad (15)$$

Further, we can correct  $C_D$  for the effect of load factor in a steady turn at bank angle  $\phi$ , by dividing  $C_L$  by  $\cos \phi$ . Setting  $\mathbf{B} = \frac{1}{\pi e AR}$  as an airframe constant, gives a new expression for  $C_D$  from Equation 12:

$$C_D = C_{D0} + \mathbf{B} \left( \frac{C_L}{\cos \phi} \right)^2 \quad (16)$$

The glide ratio, the ratio of distance traveled to height lost, or equivalently the ratio of airspeed to sink rate, is given by “L over D”:

$$\frac{L}{D} = \frac{C_L}{C_D} = \frac{v}{v_z} \quad (17)$$

and rearranging gives us an expression for sink rate  $v_z$ :

$$v_z = v \frac{C_D}{C_L} \quad (18)$$

Finally, substituting Equation 16 into Equation 18, gives the sink rate  $v_z$  in terms of  $v$  and  $\phi$ :

$$v_z(v, \phi) = v \left( \frac{C_{D0}}{C_L} + \frac{\mathbf{B}C_L}{\cos^2 \phi} \right), \quad (19)$$

and the netto variometer signal is given as:

$$\dot{e}_{net} = \dot{e} + v_z(v, \phi) \quad (20)$$

Estimation of the  $C_{D0}$ ,  $\mathbf{K}$ , and  $\mathbf{B}$  airframe-specific constants is described in Section V.

#### B. Thermal Detection

ArduSoar constantly monitors a first order low-pass-filtered version of  $\dot{e}_{net}$ :

$$\dot{e}_{filt_n} = \mathbf{T}_c \dot{e}_{net} + (1 - \mathbf{T}_c) \dot{e}_{filt_{n-1}} \quad (21)$$

Where  $\mathbf{T}_c = 0.03$ . When  $\dot{e}_{filt}$  exceeds a manually settable threshold (parameter SOAR\_VSPEED in ArduSoar’s implementation, see Table I), ArduSoar switches to the thermalling mode. Using this filtered version of the vario signal helps to remove turbulence which might otherwise trigger the algorithm.

### C. Thermal Identification and Exploitation

ArduSoar naturally interleaves these two stages: it uses observation data — variometer readings associated with GPS locations — to update its distribution over possible thermal parameters, and at the same time chooses its trajectory — a circle centered at a location  $x_0, y_0$  of radius  $\hat{R}^{th}$  — based on the thermal parameter distribution.

Recall from Equation 1 that ArduSoar’s thermal model has 4 parameters that need to be estimated:  $W^{th}$ ,  $R^{th}$ ,  $x^{th}$  and  $y^{th}$ . To simplify the math, we make the following assumption:

Given wind velocity vector  $\vec{v}^{wind}$ , aircraft velocity vector  $\vec{v}^a$ , and aircraft and thermal center locations  $\vec{p}^a$  and  $\vec{p}^{th}$  in the Earth reference frame, after time  $dt$  their locations in the Earth reference frame are  $\vec{p}^a = \vec{p}^{a'} + (\vec{v}^{wind} + \vec{v}^a)dt$  and  $\vec{p}^{th'} = \vec{p}^{th} + \vec{v}^{wind}dt$  respectively.

In other words, we assume that the aircraft and the thermal location are affected by wind in the same way. This assumption isn’t completely accurate [29], because thermals tend to move slower than the surrounding air mass. Nonetheless, for small  $dt$ , i.e., high re-estimation frequency, it is a very good approximation of reality. Moreover, it allows us to easily carry out all calculations in the aircraft’s reference frame, since, under this assumption, the relative displacement of the the aircraft and the thermal is entirely due to the aircraft’s velocity vector.

As in Hazard [17], we define the aircraft to be always at the origin of its own reference frame, so the thermal state vector to be tracked as follows:

$$\text{State vector } \mathbf{X} = \begin{bmatrix} W^{th} \\ R^{th} \\ x \\ y \end{bmatrix} = \begin{bmatrix} \text{Strength} \\ \text{Radius} \\ \text{Center distance north of aircraft} \\ \text{Center distance east of aircraft} \end{bmatrix} \quad (22)$$

Recall that state tracking with an EKF involves updating the current state distribution’s mean with a linearization of the transition function  $f$  (Equation 2) and observation function  $h$  (Equation 5). In our case, assuming that the aircraft has travelled distance  $dx$  to the north and  $dy$  to the east during a given time step, where  $dx$  and  $dy$  are both known,

$$\mathbf{X}_{k+1} = f(\mathbf{X}_k) = \mathbf{X}_k + \begin{bmatrix} 0 \\ 0 \\ -dx \\ -dy \end{bmatrix}. \quad (23)$$

Despite its apparent simplicity, the computation of  $f(\mathbf{X}_k)$  involves an important subtlety. As stated above, we aim to calculate the motion of the thermal relative to the aircraft. However, we have direct access only to the aircraft’s GPS positions  $x^{abs}, y^{abs}$  in the Earth reference frame. Since the aircraft can be affected by wind,  $dx \neq \Delta x^{abs}$  and  $dy \neq \Delta y^{abs}$  for two successive  $x^{abs}$  (resp.  $y^{abs}$ ) measurements. Rather,

$$dx = \Delta x^{abs} - v_x^{wind} \quad (24)$$

$$dy = \Delta y^{abs} - v_y^{wind}, \quad (25)$$

i.e., we need to perform *wind correction* to obtain thermal motion w.r.t. the aircraft.

Since  $f(\mathbf{X}_k)$  effectively has no process dynamics, we get

$$F = \frac{\partial f}{\partial \mathbf{X}} = \frac{\partial \mathbf{X}_{k+1}}{\partial \mathbf{X}} = \begin{bmatrix} 1 & 0 & 0 & 0 \\ 0 & 1 & 0 & 0 \\ 0 & 0 & 1 & 0 \\ 0 & 0 & 0 & 1 \end{bmatrix} = I \quad (26)$$

For the observation function, the only readings relevant to the thermal state vector that we get is vertical air velocity  $w$  at the aircraft’s position w.r.t. the thermal center, so

$$\mathbf{o} = w = h(\mathbf{X}) = W^{th} \exp\left(-\frac{x^2 + y^2}{R^{th2}}\right) \quad (27)$$

and

$$H^\top = \frac{\partial h}{\partial \mathbf{X}}^\top = \begin{bmatrix} \exp\left(-\frac{x^2 + y^2}{R^{th2}}\right) \\ \frac{2W^{th}(x^2 + y^2)}{R^{th3}} \exp\left(-\frac{x^2 + y^2}{R^{th2}}\right) \\ \frac{2W^{th}x}{R^{th2}} \exp\left(-\frac{x^2 + y^2}{R^{th2}}\right) \\ \frac{2W^{th}y}{R^{th2}} \exp\left(-\frac{x^2 + y^2}{R^{th2}}\right) \end{bmatrix} \quad (28)$$

Note the two aspects that make ArduSoar’s EKF update extra efficient:

- Due to Equation 26, covariance update (Equation 4) becomes simply  $\hat{P}_{k+1} = P_k + Q$ .
- Since our observation vector has only a single component, vertical air velocity, and  $\frac{\partial h}{\partial \mathbf{X}}$  is a  $1 \times 4$  vector (Equation 28), it follows that in Equation 6 ( $H\hat{P}_{k+1}H^\top + R$ ) is an integer and the matrix inversion during Kalman gain computation in that equation is just a division.

ArduSoar’s EKF update runs at 5Hz, giving ArduSoar a stream of thermal parameter estimates. In order to use this information to gain height, ArduSoar enters the autopilot into the LOITER mode (see the next section), in which ArduPlane ensures that the aircraft orbits a specified location in a circle of a specified radius. ArduSoar sets  $(x, y)$  from the mean thermal estimate to be the center of this circle, but setting the radius  $\hat{R}$  is less straightforward.

In theory, using the mean  $R^{th}$  estimate, ArduSoar could choose  $\hat{R}$  to strike the optimal balance between estimated lift  $\hat{R}$  meters away from the thermal center and the lift loss due to bank angle required to stay in a turn of radius  $\hat{R}$ . In practice, however, we made  $\hat{R}$  a manually settable parameter for ArduSoar, for reasons described at the end of Section V.

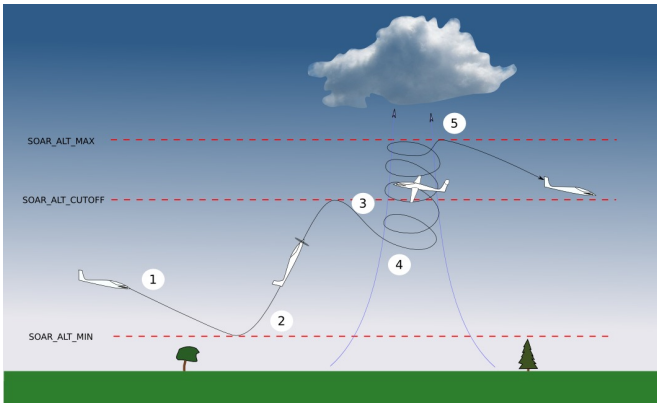


Fig. 2: ArduPlane’s typical flight profile with ArduSoar enabled. Image reproduced with permission. Source: <http://ardupilot.org/plane/docs/soaring.html>

#### D. Thermal Exit

ArduSoar constantly monitors the strength of the thermal to decide whether to exit and search for a better thermal. It is assumed that the sailplane is currently circling the thermal center at distance  $\hat{R}$ , and a lift estimate at this distance is calculated using Equation 1. The estimate is then adjusted using a constant correction factor,  $\mathbf{K}_{\text{sink}}$ , representing sink from the drag polar and bank angle. Thus, ArduSoar computes  $W^{th} \exp\left(-\frac{x^2+y^2}{\hat{R}^2}\right) - \mathbf{K}_{\text{sink}}$ , and compares it against the SOAR\_VSPEED threshold (Table I) to determine if the thermal has become too weak to continue with. Note that this exit condition doesn’t rely on the *actual* lift measurements, only on those predicted by the thermal model. This approach has the advantage over other methods [7, 14] of not being overly sensitive to the speed of the controller’s response to fluctuations in thermal size and position.

## IV. ARDUPLANE INTEGRATION

Although a soaring controller can enable an aircraft to stay aloft by extracting energy from the atmosphere, per se it lacks a lot of the useful functionality of a full-blown autopilot, including an AHRS system for estimating aircraft state, waypoint following capability, safety mechanisms such as geofencing, etc. Integrating ArduSoar into ArduPlane resulted in a flight controller for fixed-wing UAV’s that has the rich feature set of a major open-source autopilot in addition to thermalling functionality.

To integrate ArduSoar into ArduPlane, we have augmented ArduPlane with a number of parameters configurable via ground control station software such as Mission Planner [3]. These parameters are listed in Table I. Some of them, such as SOAR\_VSPEED and SOAR\_POLAR\_\*, pertain to ArduSoar itself. The rest, particularly SOAR\_ALT\_\*, control ArduSoar’s interoperation with ArduPlane.

In particular, ArduPlane has two modes relevant to ArduSoar, AUTO and LOITER:

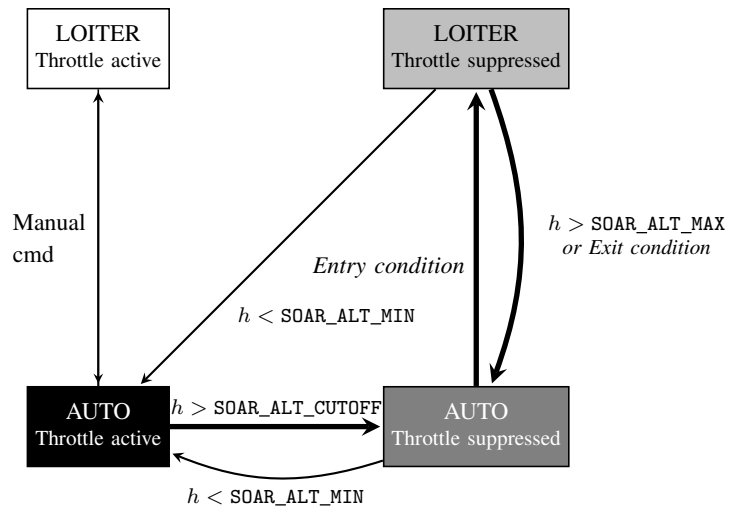


Fig. 3: State transition diagram. Normal transitions in **thick** lines.

- In AUTO mode, given a set of waypoints, a target airspeed, and several other parameters, ArduPlane’s default behavior is to fly the aircraft fully autonomously, following the specified waypoint course.
- In LOITER mode, ArduPlane’s default behavior is to orbit a point with specified GPS coordinates at a specified radius.

We modified ArduPlane’s AUTO mode to opportunistically use thermalling functionality as shown in Figure 2. If the aircraft just took off or if it descended to the altitude given by the new SOAR\_ALT\_MIN parameter (stage 1 of the flight in Figure 2), it climbs under motor to SOAR\_ALT\_CUTOFF altitude (stage 2 in Figure 2) while following pre-set waypoints. Upon reaching SOAR\_ALT\_CUTOFF, it turns off the motor and glides down at ArduPlane’s target airspeed (stage 3). During this stage, ArduSoar keeps monitoring the aircraft state. If it detects a thermal, it takes over navigational control and starts thermalling by putting the aircraft into LOITER mode (stage 4 in Figure 2). The point ArduSoar commands the aircraft to orbit is the current mean of the thermal center estimate,  $(x^{th}, y^{th})$ . The radius is given by a special ArduPlane parameter for LOITER mode called WP\_LOITER\_RAD. While thermalling, the aircraft does not follow its waypoint course and may deviate from it. It may also reach an altitude given by the SOAR\_ALT\_MAX parameter. This safety parameter terminates thermalling to prevent the aircraft from climbing too high. At that point, ArduSoar stops thermalling, gives navigational control back to ArduPlane, and the aircraft starts another motorless glide (stage 5). This process can repeat many times without any human intervention.

Several of the newly introduced parameters are meant to give the human operator the ability to experiment with ArduSoar’s behavior. Specifically, SOAR\_VSPEED determines how strong a thermal needs to be for ArduSoar to catch

it; `SOAR_MIN_THML_S` allows forcing ArduSoar to stay thermalling for a minimum time period, even if ArduSoar would otherwise decide to leave the thermal. `SOAR_MIN_CRSE_S` prevents ArduSoar from starting to thermal too soon after it exited a thermal previously, e.g., to make sure it doesn't keep entering and exiting the same thermal over and over again.

The state transition diagram of the resulting autopilot is shown in Figure 3. In AUTO mode, ArduPlane's default behavior is to use the motor and follow waypoints, so implementing ArduSoar involved overriding ArduPlane's throttle setting and navigation waypoints. Code was inserted into the main ArduPlane vehicle update functions to override the relevant variables when the soaring controller is active.

Parameter name	Description
<code>SOAR_ENABLE</code>	Enables or disables ArduSoar functionality
<code>SOAR_VSPEED</code>	A threshold for vertical air velocity that determines whether the aircraft that observes air moving upwards at <code>SOAR_VSPEED</code> should enter/exit the thermalling mode.
<code>SOAR_Q1</code>	Standard deviation of the process noise for thermal strength
<code>SOAR_Q2</code>	Standard deviation of the process noise for thermal position and radius
<code>SOAR_R</code>	Standard deviation of the observation noise
<code>SOAR_DIST_AHEAD</code>	Initial guess of the distance to the thermal center along the aircraft heading
<code>SOAR_MIN_THML_S</code>	Minimum time the aircraft should keep trying to soar once it has entered the thermalling mode (LOITER), in seconds
<code>SOAR_MIN_CRSE_S</code>	Minimum time the aircraft should avoid entering the thermalling mode (LOITER) after it last exited it, in seconds
<code>SOAR_POLAR_CDO</code>	Polar curve parameter (see eq. (12))
<code>SOAR_POLAR_B</code>	Polar curve parameter (see eq. (16))
<code>SOAR_POLAR_K</code>	Polar curve parameter (see eq. (15))
<code>SOAR_ALT_MIN</code>	The minimum altitude at which soaring or off-motor gliding is allowed, in meters. If the aircraft descends to <code>SOAR_ALT_MIN</code> , it turns on the motor and starts climbing in AUTO mode.
<code>SOAR_ALT_CUTOFF</code>	The altitude, in meters, at which the aircraft turns off the motor after a climb from <code>SOAR_ALT_MIN</code> (or from the ground) and starts gliding in AUTO mode, trying to detect thermals.
<code>SOAR_ALT_MAX</code>	The maximum altitude, in meters, that the aircraft is allowed to reach. Upon reaching it, the aircraft exits the thermalling mode if necessary and starts a glide in AUTO mode.

TABLE I: Parameters of the ArduSoar controller settable in ArduPlane.

The main logic of the controller is divided into modules:

- 1) `soaring.cpp` provides a single function, `update_soaring()`, that is called by the task scheduler at 50Hz. Depending on the current flight mode this function updates the soaring controller and checks for required changes to flight mode and navigation target. It exists in the main ArduPlane namespace, allowing it to set the required variables directly.
- 2) `AP_SoaringController.cpp` provides the main controller logic, including methods to update the thermal estimator and the variometer, calculation of the navigation target

and methods that trigger flight mode changes.

- 3) `Variometer` provides the total energy rate estimate from height, airspeed and roll measurements.
- 4) `ExtendedKalmanFilter` provides the thermal parameter estimate from the total energy rate estimate and the aircraft position.

At any instant the system has two primary state variables that determine its behaviour. *Flight mode* is an ArduPilot feature that selectively enables control features. *Throttle suppressed* is a flag within the soaring controller that determines whether the throttle signal is forced to zero. The transitions between the states are triggered by `update_soaring()` based on altitude and thermal parameter estimates. The transition diagram is illustrated in Figure 3.

A number of other interactions were required between ArduSoar and ArduPlane. For example, the rapid changes of operating regime when switching between *throttle suppressed* and *throttle active* states require large changes in trim pitch angle. This mandated resetting the pitch integrator on state transitions to avoid overshoots.

## V. FLIGHT TESTING

Flight testing was conducted in two phases: airframe characterization, in which the polar curve parameters of a Parkzone Radian Pro, a popular remote-controlled sailplane, were estimated; and controller tuning, in which key parameters affecting the performance of ArduSoar were adjusted.

The Radian Pro was equipped with a 3DR Pixhawk flight controller hardware (32-bit ARM processor, 256KB RAM, 2MB flash memory, 168MHz clock speed), a 3DR GPS and compass, a 3DR pitot/static tube and a sensor, a 3DR 915MHz telemetry radio, and a FrSky X8R receiver. The remote pilot could intervene at any point using a FrSky X9D+ 2.4GHz transmitter. Power was provided by a single 3-cell 1300 mAh LiPo battery. The equipment diagram is shown in Figure 4.

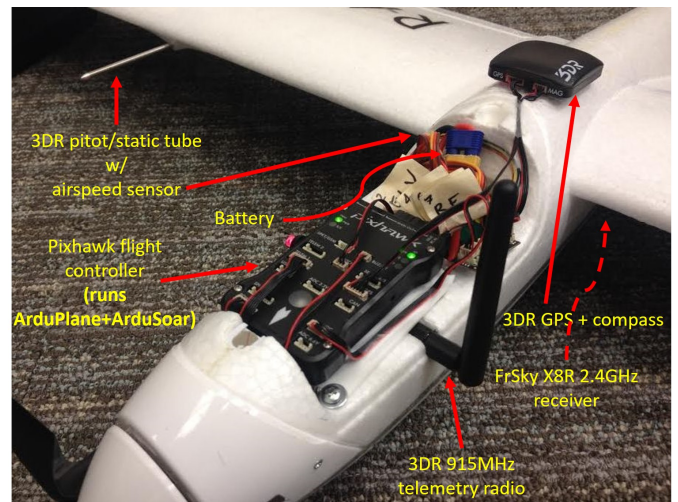


Fig. 4: Radian Pro with its electronic equipment (the canopy is temporarily removed)

The polar curve was estimated by conducting test glides in calm air. ArduPlane’s AUTO mode was used to track a target airspeed around a triangular course, for a range of target airspeeds. The descent rate was measured for each, and parameters SOAR\_POLAR\_B and SOAR\_POLAR\_CDO were fitted to the resulting data using a least squares fit of Equations 12 and 16. SOAR\_POLAR\_K was determined directly from the wing dimensions and weight of the Radian Pro, and  $\rho = 1.225 \text{ kg m}^{-3}$  was assumed since all flight testing was conducted near sea level.

Controller tuning required deriving estimates of variometer measurement noise  $R = [\text{SOAR\_R}^2]$ , initial state values and variances  $x_{\text{init}}$  and  $P_{\text{init}}$  and state process noise

$$Q = \begin{bmatrix} \text{SOAR\_Q1}^2 & 0 & 0 & 0 \\ 0 & \text{SOAR\_Q2}^2 & 0 & 0 \\ 0 & 0 & \text{SOAR\_Q2}^2 & 0 \\ 0 & 0 & 0 & \text{SOAR\_Q2}^2 \end{bmatrix} \quad (29)$$

(see Table I). These were tuned largely by analysis of filter performance during thermal encounters. The underlying model assumes a static updraft distribution, so SOAR\_R captures variations in vario readings due to actual measurement noise, unmodelled aircraft dynamics and turbulence. SOAR\_R was therefore taken as the variance in reading during circling flight in turbulent air.

In the initial seconds of thermal encounter it is essential to maintain uncertainty in position estimates  $x^{th}$  and  $y^{th}$ . This allows movement of the estimated thermal center and is achieved by large initial variances of  $x^{th}$  and  $y^{th}$ . The aircraft will follow this estimated center, yielding additional information that rapidly localizes the thermal center and reduces the state variances. The initial variance of  $W^{th}$  and  $R^{th}$  also affect the ability of  $x^{th}$  and  $y^{th}$  to change, and so are selected relatively smaller.

After the initial filter transients, the balance between SOAR\_R and the elements of  $Q$  determines the steady-state magnitude of the elements of the state covariance matrix  $P$ . For a given SOAR\_R, small values of  $Q$  lead to low state covariances. These small values in  $P$  give a small response to innovations; the states become almost constant over time. Conversely, large values of  $Q$  increase state uncertainty so  $P$  is larger. This gives the filter the ability to refine the thermal position estimate.

The elements of  $Q$  are selected to give good filter response characteristics in steady-state thermalling. The strength and radius estimates should change slowly (on the order of the period of thermal orbit) relative to the position estimates.

As mentioned previously, despite the EKF providing ArduSoar with estimates of the thermal radius, we opted to set the radius  $\hat{R}$  that ArduSoar uses in LOITER mode to a manually specified parameter, WP\_LOITER\_RAD. We did this because for thermals at low altitudes where we conducted our test flights, we observed a large variance in the  $R^{th}$  estimates, indicating that they were unreliable. Moreover, we observed large covariances between  $W^{th}$  and  $R^{th}$  estimates, indicating that,

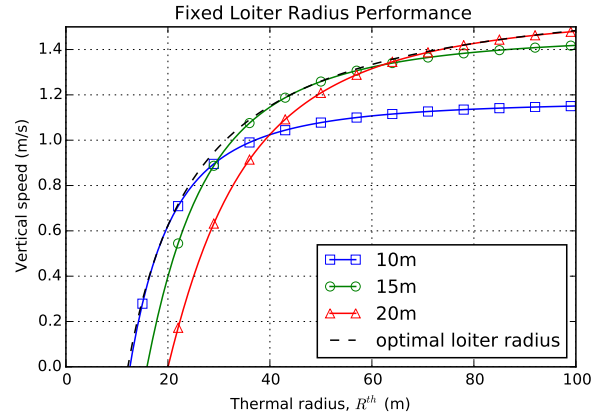


Fig. 5: Simulation results showing the trade-offs in soaring performance from using three different fixed loiter radii over a wide range of thermal sizes ( $R^{th}$ ) with  $W^{th} = 2.5 \text{ m s}^{-1}$ , compared to using the optimal loiter radius for that thermal size.

at least for the irregular thermals at low altitudes, ArduSoar had difficulty distinguishing between strong narrow thermals and weak large ones. This is not surprising given ArduSoar’s lack of exploration of the thermal — once it is confident of the center location, it orbits it and doesn’t attempt to reduce the variance of its  $W^{th}$  and  $R^{th}$  estimates. An exploration strategy such as deliberately varying the orbit radius could alleviate this problem.

At the same time, we observed that the smallest turn radius that a Radian Pro can reliably maintain in LOITER mode, 15m, works well across a wide range of thermals. Figure 5, based on simulated thermals, shows the trade-off in soaring performance with the choice of loiter radius. Using a small loiter radius extends performance to smaller thermals but at the expense of performance in large thermals. Additionally, trying to orbit tightly at speeds close to the stall speed, where soaring performance is best, can be challenging for the autopilot. For the Radian Pro glider a radius of 15 m at an airspeed of 9 m/s provides a good compromise. We found that setting the loiter radius too tightly resulted in occasional tip stalls leading to dangerous flat spins, which required manual intervention to recover.

## VI. RELATED WORK

Besides autonomous dynamic soaring and soaring in thermals, researchers have considered many other ways of extracting energy from the atmosphere to maintain flight, such as exploiting gusts [22], wind fields [24], and orographic lift [21, 16]. Of these, ArduSoar can and successfully has been used for soaring in orographic lift, generated by wind blowing into a vertical obstacle such a tree line or a hill and forcing the air to move upwards. Although the true shape of a rising air mass in this case can be almost arbitrary and is certainly far from a column, ArduSoar’s strategy of circling in order to stay within the airmass is a valid approach to exploiting this kind of

lift. Techniques for flight path planning to increased endurance due to natural lift sources has also received attention in the literature [15, 24, 11, 12, 13], but is far from the topic of our work.

Among previously proposed autonomous soaring approaches, those by Wharington et al [30, 31], Allen and Lin [7], and Edwards [14] are the closest to ours. All three use a Gaussian thermal model first proposed in [31] and later modified by Allen and Lin [7]. The difference lies in the set of hypotheses each approach maintains, and its thermal exploitation strategy. In their simulation scenarios, Warrington et al [30, 31] maintain a fixed grid of candidate thermal center locations over the flight area, and identify the node where the thermal parameter fit is best, as the center. A control strategy developed with the help of reinforcement learning (RL) [28], was trained using a simple simulator. Convergence of the solver was slow prohibiting any practical implementation. Allen and Lin [7] place the thermal center at the centroid of the recent history of  $\hat{e}$  observation locations, each weighted by the square of its measurement. Thermal radius is fitted to the observations using gradient descent. The thermal is then exploited using a controller based on a form of Reichmann rules [7, 27]. Edwards [14] mitigated the problem of biased thermal center estimation in [7] to the inside of a turn, by augmenting Allen's centroid locator with a surrounding grid of candidate thermal locations (similar to [30]), but makes grid scale and placement adaptive. An evolutionary search recursively refines the thermal parameters by choosing the grid point with the best fit to the observation history at each step, using least squares. Edwards and Silberberg [15] also presents a weighted least squares method to simultaneously fit the all parameters of generalized ellipsoidal thermal model, without the need of a search grid. However in flight testing the method was found to be unreliable and sensitive to observation noise. Bird and Langelaan [10], presents a method to map the vertical wind field around the sailplane by fitting the weights of a parametric spline surface to observations using an extended kalman filter. To exploit the arbitrary uplift map, a contour solver is used to extract the optimal lift isotherm along which the sailplane is then guided, augmented with a sinusoidal dither signal to promote exploration and refinement of the map. Simulation results show no significant performance improvement over the previously described controllers even for irregular shaped thermals. Reddy et al. [26], like Wharington [30], employ an RL method to learn a policy, however they utilize the much more detailed thermal simulation based on Rayleigh-Bénard convection. Like Wharington [30]'s and other RL based approaches, theirs requires a random RL trial restart capability, which is far too impractical to conduct in the real world, limiting training to simulation only. Without flight testing, it is not clear how well the learnt control strategies would carry over to the real world. On the other hand, Edwards [14] conducted a live flight test of his controller and kept a sailplane airborne for 5.28 hours along a closed course. During the tests, thermal centering ran on a laptop on the ground; due to its use of adaptive grid for thermal

hypotheses, Edwards's approach is still too expensive for a computationally constrained device as a Pixhawk.

An efficient alternative means of thermal identification for simulated autonomous thermalling is by Hazard [17]. It derives a UKF-based thermal tracking approach and evaluates its performance at determining a thermal's parameters assuming various open-loop environment exploration policies, such as flying a horizontal circular or sinusoidal pattern. Our work uses several elements of Hazard's work, particularly the thermal model and insights regarding tracking it using a Kalman filter variant.

In another implementation [19], an EKF estimator is used to identify thermal dynamics. Its state variables are thermal strength, radius, distance from aircraft and bearing to aircraft. State dynamics are introduced to cause a decay in the thermal strength state. The estimation is separated into two 2-variable EKFs, because the dynamics of the thermal strength and radius are decoupled from the position states. The formulation can be executed iteratively on an embedded autopilot. This differs from our approach in that the more complex state dynamics increase computational complexity and the decoupled estimation approach does not capture the coupling between the *uncertainties* in the states. These coupling terms are captured as off-diagonal terms in the covariance matrix of our 4-variable estimator.

## VII. CONCLUSIONS

This paper has presented ArduSoar, an embedded thermal soaring controller that has been implemented and tested in the codebase of a popular open-source autopilot for fixed-wing UAVs called ArduPlane. ArduSoar is based on a 4-variable estimator that uses an extended Kalman filter with trivial state dynamics to achieve a computational cost low enough for ArduSoar to be executable on highly resource-constrained drone autopilot hardware such as Pixhawk or even APM. The implementation demonstrates good performance and has been used by several research groups as well as many individuals for leisure, research and commercial purposes.

**Acknowledgements.** We would like to thank Peter Braswell for making available his soaring controller code that ArduSoar's implementation is derived from.

## REFERENCES

- [1] Ardupilot project website. <http://www.ardupilot.org>, . Accessed: 2018-02-10.
- [2] ArduPlane, . URL <http://ardupilot.org/plane/index.html>.
- [3] Mission planner. URL <http://ardupilot.org/planner/>.
- [4] Pixhawk project website. <https://pixhawk.org/>. Accessed: 2018-02-10.
- [5] Raspberry pi project website. <http://raspberrypi.org/>. Accessed: 2018-02-10.
- [6] M. Allen. Updraft model for development of autonomous soaring uninhabited air vehicles. In *Proc. of the 44th AIAA Aerospace Sciences Meeting and Exhibit*, 2006. doi: <https://doi.org/10.2514/6>.

- 2006-1510. URL <https://ntrs.nasa.gov/archive/nasa/casi.ntrs.nasa.gov/20060004052.pdf>.
- [7] M.J. Allen and V. Lin. Guidance and control of an autonomous soaring UAV. Technical report, 2007. URL <https://ntrs.nasa.gov/archive/nasa/casi.ntrs.nasa.gov/20070022339.pdf>.
- [8] J. D. Anderson. Introduction to flight, 1989.
- [9] J. J. Bird, J. W. Langelaan, C. Montella, J. Spletzer, and J. Grenestedt. Closing the loop in dynamic soaring. In *Proc. of the 54th AIAA Guidance, Navigation and Control Conference and Exhibit*, 2014.
- [10] John Bird and Jack Langelaan. Spline mapping to maximize energy exploitation of non-uniform thermals. *Technical Soaring*, 37(3):38–44, 2013.
- [11] A. Chakrabarty and Jack W. Langelaan. Energy-based long-range path planning for soaring-capable uavs. *Journal of Guidance, Control and Dynamics*, 34(4):1002–1015, 2011.
- [12] J. J. Chung, N. R. J. Lawrance, and S. Sukkarieh. Learning to soar: Resource-constrained exploration in reinforcement learning. *The International Journal of Robotics Research*, 34(2):158–172, 2015.
- [13] N. T. Depenbusch, J. J. Bird, and Jack W. Langelaan. The autosoar autonomous soaring aircraft part 2: Hardware implementation and flight results. *Journal of Field Robotics*. doi: 10.1002/rob.21747. URL <http://onlinelibrary.wiley.com/doi/10.1002/rob.21747/full>.
- [14] D. Edwards. Implementation details and flight test results of an autonomous soaring controller. In *Proc. of the 46th AIAA Guidance, Navigation and Control Conference and Exhibit*, 2008. doi: <https://doi.org/10.2514/6.2008-7244>. URL <http://citeseerx.ist.psu.edu/viewdoc/download?doi=10.1.1.559.4025&rep=rep1&type=pdf>.
- [15] D. J. Edwards and L. M. Silberberg. Autonomous soaring: The montague cross-country challenge. *Journal of Aircraft*, 47(5):1763–1769, 2010. doi: <https://doi.org/10.2514/1.C000287>. URL <https://arc.aiaa.org/doi/abs/10.2514/1.C000287>.
- [16] A. Fisher, M. Marino, R. Clothier, S. Watkins, L. Peters, and J. L. Palmer. Emulating avian orographic soaring with a small autonomous glider. *Bioinspiration & Biomimetics*, 11(1), 2016. URL <http://stacks.iop.org/1748-3190/11/i=1/a=016002>.
- [17] M. W. Hazard. Unscented kalman filter for thermal parameter identification. In *Proc. of the 48th AIAA Aerospace Sciences Meeting and Exhibit*, 2010.
- [18] L. P. Kadanoff. Turbulent heat flow: structures and scaling. *Physics Today*, 54(8):34–39, 2001.
- [19] A. M. Kahn. Atmospheric thermal location estimation. *Journal of Guidance, Control and Dynamics*, 40, 2017.
- [20] R.E. Kalman. A new approach to linear filtering and prediction problems. *Transactions of the ASME—Journal of Basic Engineering*, 82(Series D):35–45, 1960.
- [21] J. W. Langelaan. Long distance/duration trajectory optimization for small UAVs. In *Proc. of the 47th AIAA Guidance, Navigation and Control Conference and Exhibit*, 2007.
- [22] J. W. Langelaan. Gust energy extraction for mini- and micro- uninhabited aerial vehicles. In *Proc. of the 46th AIAA Aerospace Sciences Meeting and Exhibit*, 2008.
- [23] N. R. J. Lawrance and S. Sukkarieh. A guidance and control strategy for dynamic soaring with a gliding uav. In *Proc. of IEEE International Conference on Robotics and Automation (ICRA)*, pages 3632–3637, 2009. URL <http://ieeexplore.ieee.org/abstract/document/5152441/>.
- [24] N. R. J. Lawrance and S. Sukkarieh. Path planning for autonomous soaring flight in dynamic wind fields. In *Proc. of IEEE International Conference on Robotics and Automation (ICRA)*, pages 2499–2505, 2011. URL <http://ieeexplore.ieee.org/abstract/document/5979966/>.
- [25] P. Oettershagen, A. Melzer, T. Mantel, K. Rudin, T. Stastny, B. Wawrzacz, T. Hinzmann, S. Leutenegger, K. Alexis, and R. Siegwart. Design of small hand-launched solar-powered uavs: From concept study to a multi-day world endurance record flight. volume 34, pages 1352–1377, 2017. doi: 10.1002/rob.21717. URL <http://dx.doi.org/10.1002/rob.21717>.
- [26] G. Reddy, A. Celani, T. J. Sejnowski, and M. Vergassola. Learning to soar in turbulent environments. In *Proc. of the National Academy of Science (PNAS)*, 2016.
- [27] H. Reichmann. *Cross-Country Soaring*. 7th ed. edition, 1993.
- [28] R. S. Sutton and A. G. Barto. *Reinforcement Learning: An Introduction*. MIT Press, 1998.
- [29] J. W. Telford. Convective plumes in a convective field. *Journal of the Atmospheric Sciences*, 27(3):347–358, 1970.
- [30] J. Wharington. *Autonomous Control of Soaring Aircraft by Reinforcement Learning*. Doctorate thesis, Royal Melbourne Institute of Technology, Melbourne, Australia, 1998.
- [31] J. Wharington and I. Herszberg. Control of a high endurance unmanned air vehicle. In *Proc. of the 21st ICAS Congress*, 1998.